On the Atmospheric Boundary Layer over the Equatorial Front*

STEVEN P. ANDERSON

Department of Physical Oceanography, Woods Hole Oceanographic Institution, Woods Hole, Massachussets

17 April 2000 and 21 August 2000

ABSTRACT

This paper presents surface meteorological data and boundary layer profiles from a single meridional transect across the equator along 125°W collected during the Pan American Climate Study mooring cruise in September of 1998. These observations are unique because they occurred at the start of a cold event in the eastern tropical Pacific when the SST gradients along the equatorial front were near their climatological maximum. In addition to the anomalous cold conditions encountered near the equator, an added benefit of this limited study is the relatively high station resolution across the front. The meridional minimum in SST, and center of the cold tongue, was 20.9°C and occurred at 0.4°N. An equatorial front was located to the north where SST increased linearly to 25.5°C at 2.0°N. The atmospheric boundary layer (ABL) was stable over the cold tongue. An unstable ABL developed over the warm side of the front in less than 55 km. The unstable ABL was found at two more stations over the warm side of the front and had a height of 350–450 m. Collocated with the formation of the unstable ABL was a rapid acceleration of the surface wind field. These observations are consistent with the hypothesis that the surface wind field is modulated by stability-dependent boundary layer effects. These observations also suggest that the spatial scale of the surface wind acceleration is less than the spatial scale of the SST front.

1. Introduction

The sea surface temperature (SST) field in the eastern tropical Pacific is usually marked by a ''cold tongue'' of water that extends westward from South America along the equator. SST fronts exist between this cold tongue and the regions to the north and south. The strength of the cold tongue and associated fronts change seasonally and interannually (Mitchell and Wallace 1992). The winds in this region are typically southeasterly. However, the strength and spatial distribution of the surface winds (in particular the wind divergence and curl) have been shown to be closely tied to the frontal location and strength. The modulation of the surface wind field by the SST provides a potential mechanism for two-way air–sea coupling since the wind is a key parameter in governing the air–sea transfer of heat and momentum.

The analysis of the Comprehensive Ocean–Atmosphere Dataset (COADS) by Wallace et al. (1989) suggests stability-dependent boundary layer effects on surface wind may be a mechanism of air–sea coupling in this region. The large-scale meridional SST gradients are thought to set up a meridional pressure gradient that drive low-level southerly winds (Lindzen and Nigam 1987). Over the cold tongue, the stable atmospheric boundary layer (ABL), combined with the surface drag, acts to reduce momentum transfer down to the surface and thus reduces the surface winds compared with those found aloft. Over the warm side of the equatorial front, convection destabilizes the boundary layer and allows for turbulent mixing of momentum down to the surface resulting in an increase in the surface winds. The analysis of Wallace et al. (1989) shows that this effect will be most dramatic during the cold season and particularly strong during cold events. They also suggest that the coupling may occur at timescales shorter than they could resolve from the COADS data.

Extensive direct observations of the ABL in the eastern equatorial Pacific were collected in 1989 during the Equatorial Pacific Ocean Climate Studies (EPOCS) mooring deployment cruise (Bond 1992) and in 1979 during the First Global Atmospheric Research Program Global Experiment (FGGE; Yin and Albrecht 2000). The EPOCS observations were collected during typical cold-season conditions in the eastern Pacific and included direct observations of the vertical structure of the air temperature, humidity, and wind from the surface up through the boundary layer and covered a larger area. Bond (1992) analyzed the EPOCS data and found that the ABL was slightly stable over the cold tongue be-

* Woods Hole Oceanographic Institution Contribution Number 10183.

Corresponding author address: Steven P. Anderson, Dept. of Physical Oceanography, MS#29, Woods Hole Oceanographic Institution, Woods Hole, MA 02556.
E-mail: sanderson@whoi.edu

tween 2°S and 1°N and his observations were consistent with the hypothesis that the increased static stability found over the cold tongue supported enhanced low-level wind shears. Recently, Yin and Albrecht (2000) completed an extensive review of spatial variability of the ABL in the eastern Pacific using the FGGE data. The FGGE observations were collected during weak cold tongue conditions. Despite the relative weakness of the equatorial front, Yin and Albrecht (2000) found that in the eastern Pacific, there was a larger frequency of unstable atmospheric soundings north of the equatorial front than south of the front.

Although these comprehensive observational studies provide a view of the large-scale variability of the ABL, they do not provide insight into the coupling of the ABL to the underlying SST fields on short time-and space scales. Westward-propagating tropical instability waves (TIW) with wavelengths of 1000 km and periods of 20–30 days are known to perturb the equatorial front (Legeckis 1977; Pullen et al. 1987). Hayes et al. (1989) were the first to document the link between the surface wind and SST variability associated with tropical instability waves using mooring data. However, the sparsely spaced mooring data was limited and did not allow for a full resolution of the temporal and spatial variability. Deser et al. (1993) provided a glimpse at the spatially and temporally evolving coupled ocean and atmosphere by examining the SST and low cloud cover derived from satellite observations. They were able to show that the maximum in low clouds was located over the equatorial front during a cold season when the front and cross-frontal winds were strong, and both the front and collocated low cloud maximum were modulated by the tropical instability waves.

The recent analyses from satellite scatterometer surface wind data in conjunction with simultaneous satellite SST data has provided a clear picture of the coevolving SST and surface wind fields associated with the tropical instability waves (Xie et al. 1998; Chelton et al. 2001). Xie et al. (1998) were the first to analyze the time–space structure of the TIW-induced wind fluctuations. However, the study by Chelton et al. (2000) is unique in that it takes advantage of not only a high-resolution wind field derived from the National Aeronautics and Space Administration's Quick Scatterometer (QuikSCAT) satellite scatterometer but also a new technique using Tropical Rainfall Measuring Mission Microwave Imager (TMI) to image the SST field through clouds (Chelton et al. 2001). Chelton et al. (2000) are the first to provide a comprehensive analysis of the temporal and spatial structure of the wind stress and SST fields. The dynamical implications of a collocated wind divergence and curl maxima along the equatorial front are likely complicated and remain unresolved (Chelton et al. 2000).

This paper reports on a set of observations collected during a single transit across the equatorial front. These observations are unique because they occurred at the start of a cold event in the eastern tropical Pacific when the SST gradients along the equatorial front were near their climatological maximum. In addition to the anomalous cold conditions encountered near the equator, an added benefit of this limited study is the relatively high station resolution across the front. The data show clear evidence of the transition of a stable to unstable ABL and a coincident acceleration of the surface winds moving from the cold side to the warm side of the front.

The data were collected along 125°W in September of 1998 on board the R/V *Melville* during the final mooring recovery cruise for the National Oceanic and Atmospheric Administration's Pan American Climate Study (PACS) Pilot Mooring Program (Ostrom et al. 1999). The front in September of 1998 was twice as strong as the front Bond (1992) encountered in October–November of 1989 that only ranged from 24° to 26°C between the equator and 2°N. These new observations include surface meteorological data and boundary layer soundings of air temperature and humidity. A description of the instrumentation and measurement program is provided in section 2. The observational results are presented in section 3. A discussion of the results is in section 4, and final conclusions are in section 5.

2. Measurement program

The data presented in this study were collected during the final PACS mooring servicing cruise of the R/V *Melville* (Ostrom et al. 1999). The R/V *Melville* left San Diego on 6 September 1998, and made a transit down to 10°N, 125°W to recover the first mooring. The R/V *Melville* then followed 125°W south to 2.5°S to recover the second mooring. After recovering the southern mooring, the R/V *Melville* returned to San Diego on 30 September 1998. The data reported on here were collected during the transit from 8°N to 2.5°S along 125°W. The ship started the transect at 8°N at 2000 UTC 15 September 2000, crossed the equator at 0500 UTC 18 September 2000, and arrived at 2.5°S at 2330 UTC 18 September 2000.

The cruise track is overlaid on the SST field for 17 September 1998 derived from the TMI (Chelton et al. 2000; D. Chelton 2000, personal communication) in Fig. 1. The cold tongue of water can clearly be seen extending out from South America and along the equator. A series of tropical instability waves can be seen in the SST fields as they perturb the tropical fronts that define the cold tongue. These waves have wavelengths of 1000–2000 km and a large northward displacement can be seen near 118°W. At 125°W, the center of the cold tongue is centered just north of the equator. The north wall of the cold tongue is rotated by approximately 15°, thus the transect crossed the front almost perpendicularly. The SST gradients are stronger on the northern side than on the southern side of the front. Along 125°W, the warmest SSTs are found north of 5°N, and the ITCZ was located between 5° and 10°N at this time.

The R/V *Melville* shipboard Improved Meteorologi-

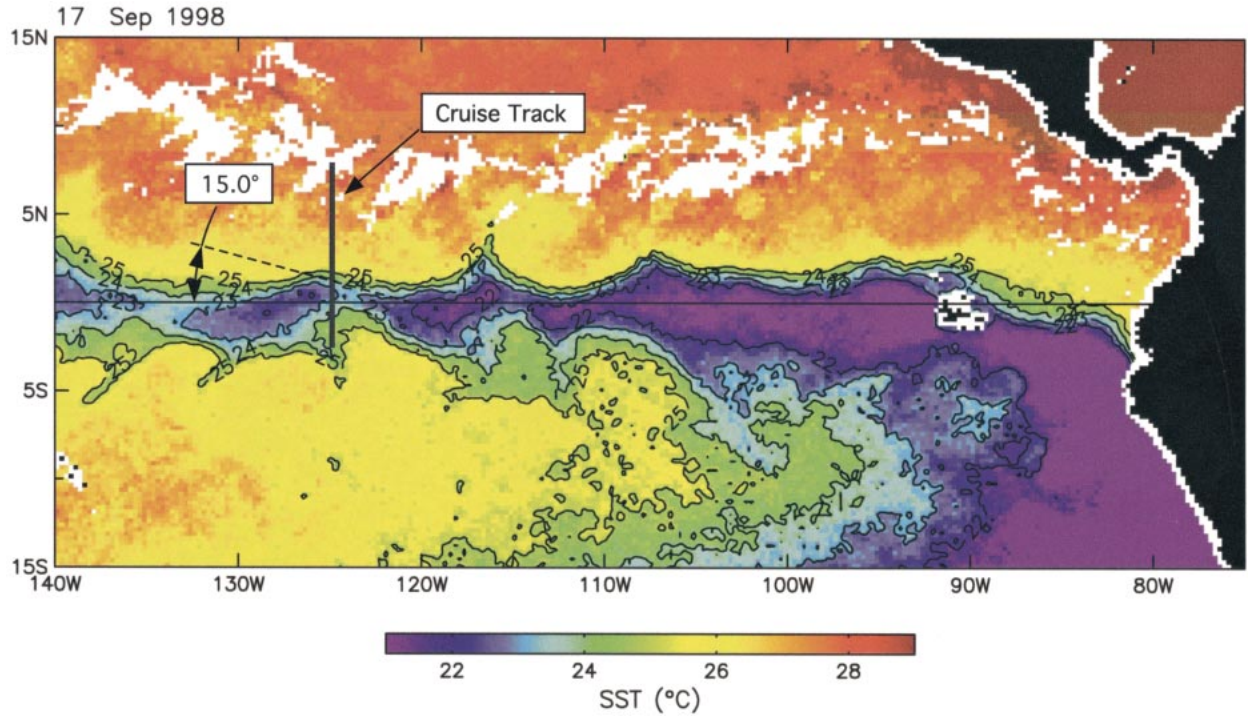

FIG. 1. Sea surface temperature field in the eastern tropical Pacific for 17 Sep 1998. These fields were derived from the TMI, have a spatial resolution of 46 km, and are a 3-day average. The location of the transect is indicated on the figure (courtesy of D. Chelton and M. Schlax based on TMI data provided by F. Wentz and C. Gentemann of Remote Sensing Systems, Inc.).

cal Instrument (IMET) system records wind speed, wind direction, air temperature, relative humidity, and barometric pressure. The measurement height is approximately 14 m. Data from this system are sampled and recorded every minute by the shipboard computer system. In addition to the standard shipboard equipment, we deployed a second IMET relative humidity and air temperature module on the bow mast as a backup. This system was connected to an Onset Computer Corporation model TT-7 data logger to record 1-min data. The R/V *Melville* also has a thermosalinograph that monitors surface temperature and salinity at an intake near the bow dome; however, this system failed shortly after leaving port. There is a secondary SST system that monitors the engine intake temperature that performed continuously. SST data from this instrument were compared with the CTD and bucket temperature to assure it provided an accurate representation of the bulk SST.

TABLE 1. Boundary layer sounding station information.

Time	Lat	Long	SST (°C)	Stability* (°C)
1552 UTC 17 Sep 1998	1.75°N	125.00°W	24.7	0.8
1952 UTC 17 Sep 1998	1.33°N	125.00°W	23.4	0.3
2346 UTC 17 Sep 1998	0.80°N	125.00°W	21.7	−0.4
0351 UTC 18 Sep 1998	0.28°N	125.00°W	21.0	−0.6
0750 UTC 18 Sep 1998	0.13°S	125.00°W	21.6	−0.2
1218 UTC 18 Sep 1998	0.68°S	125.00°W	22.6	0.0

* Difference between the surface temperature and the observed potential temperature at 14 m above the surface.

Absolute surface wind vectors in true earth coordinates were computed during postcruise processing using 1-min data from the R/V *Melville's* global positioning system and gyro. Wind data during times of rapid acceleration and deceleration were removed prior to analysis. All surface meteorological data were then averaged into 0.05° latitudinal bins for analysis. The absolute wind speed has an uncertainly of approximately ± 1.1 m s^{-1}, assuming wind and ship speed uncertainties of ± 0.5 m s^{-1}.

The Vaisala, Inc., RS-80 radiosondes were initialized within the laboratory, attached to helium-filled meteorological balloons, and released from the stern of the ship. The air temperature, wet-bulb temperature, and pressure were telemetered by 401-MHz signal and were received by an antenna mounted on the CTD hangar roof at middeck. Data were recorded with a Vaisala, Inc., Sounding Processor PP-15 and computer located in the main laboratory. A total of six soundings, with approximately 15-m vertical resolution, were collected while going across the equatorial front. A summary of sounding station information is provided in Table 1.

3. Observations and results

Several different boundary layer regimes can be identified in the surface meteorological data from the transit

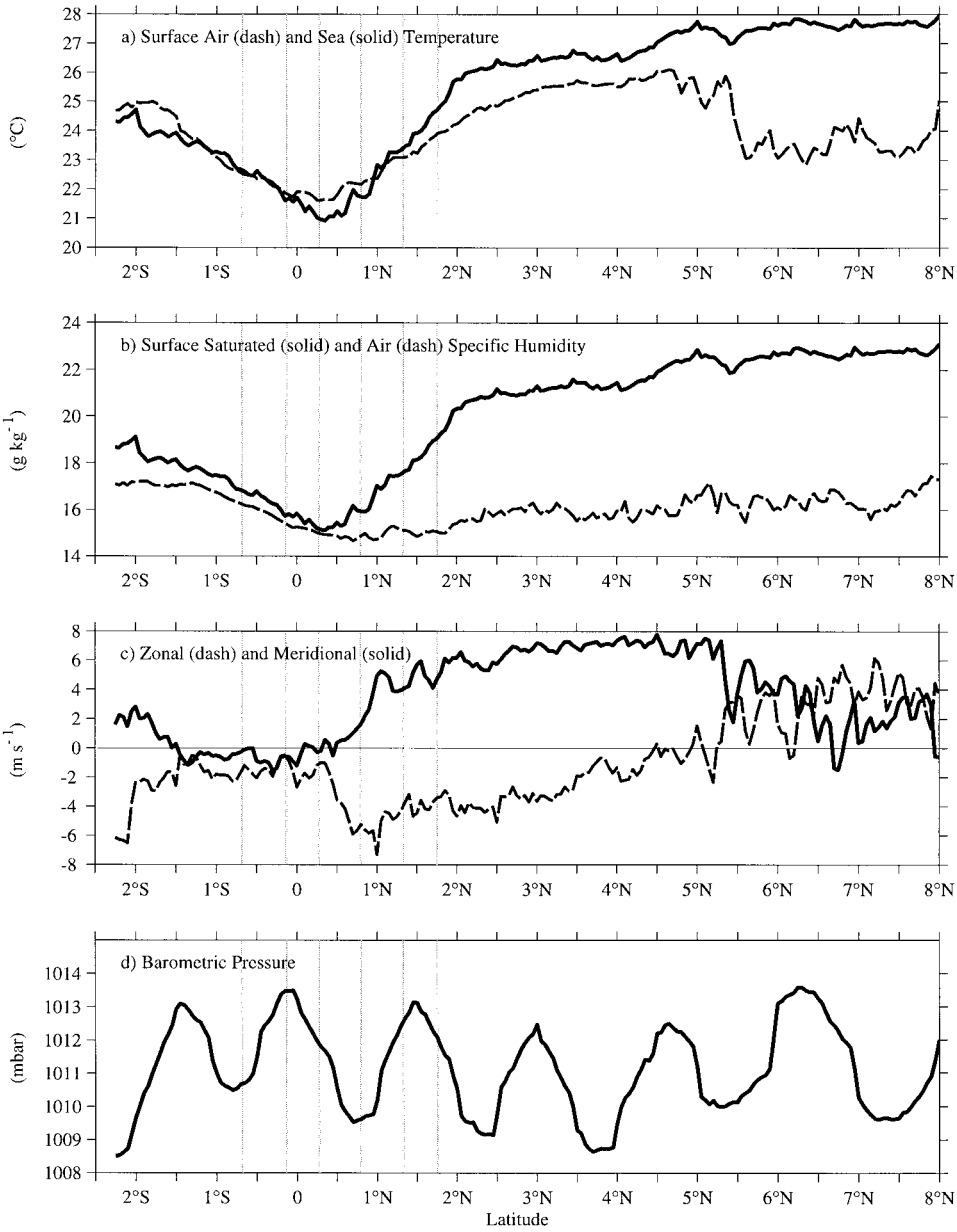

FIG. 2. Surface meteorological data along 125°W. Data were collected by the R/V *Melville* during transit along 125°W from 8°N to 2.5°S and were averaged into 0.05° bins prior to plotting. (a) Sea surface temperature and surface air temperature, (b) surface saturated specific humidity and near-surface humidity, (c) zonal and meridional wind components, and (d) barometric pressure. Vertical gray lines indicate the locations of the sounding stations.

along 125°W (Fig. 2). These new observations from a single transect are in surprisingly good agreement both qualitatively and quantitatively with the cold-year/cold-season climatological conditions found by Wallace et al. (1989). They report a minimum SST of 21°C at the equator that increases sharply to the north, reaching 25°C at 2.5°N. This observation is collocated with an increase in the meridional winds from 2 to 5 m s^{-1} and with a change in air–sea temperature difference from 0.3° to 1.2°C. In addition, they report a steady meridional pressure decrease of 2 hPa from the southern side of the cold tongue to the far side of the north wall at 5°N.

The warmest SST and largest air–sea temperature and humidity differences along 125°W in September of 1998 were found north of 5°N under the ITCZ. The surface winds under the ITCZ were variable and out of the northeast. A low cloud base and frequent rain were ob-

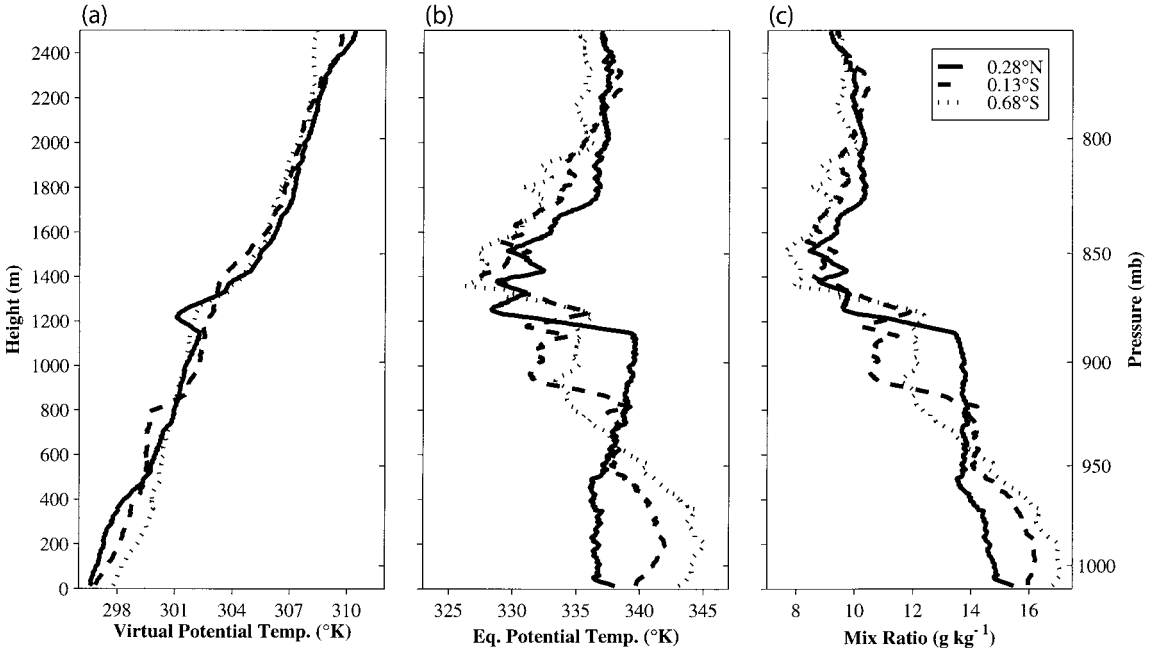

FIG. 3. Boundary layer profiles from the cold side of the equatorial front. (a) Virtual potential temperature, (b) equivalent potential temperature, and (c) mixing ratio for three profiles located along 125°W at 0.28°N, 0.13°S, and 0.68°S.

served through this region. The boundary layer in this regime is very unstable and convective. Between 5° and 2°N, clear skies were observed, with persistent 8–10 m s^{-1} winds out of the south-southeast. The air temperature warmed, air–sea temperature difference ranged from 1° to 2°C, and the humidity remained near 16 g kg^{-1}. The boundary layer in this regime is unstable and has reduced spatial variability. A near-neutral boundary layer and winds below 3 m s^{-1} are found from the equator south to 2°S where the SST slowly increases toward the south.

The north wall of the cold tongue was found just north of the equator. The coldest SST, 20.9°C, was found at 0.4°N, and the SST increased linearly with latitude to 2°N, reaching a value of 25.5°C. This is a region of transition from a stable ABL found from the equator to approximately 1.0°N to an unstable ABL on the warm side of the front. The minimum observed air temperature is collocated with the SST minimum, and, at the center of the cold tongue, the air temperature is warmer than the SST by 0.7°. At this location, the air–surface humidity difference is near zero. North of 1.0°N, the sea–air temperature and humidity differences grow and indicate unstable conditions. The surface wind field accelerates from below 2 to more than 7 m s^{-1} out of the southeast between the center of the cold tongue and 1.0°N.

The dominant signal in the surface pressure signal is the semidiurnal atmospheric tide. No attempt has been made to remove this tidal signal. However, the data suggest a relatively steady decrease in pressure from the southern wall of the cold tongue at l°S to the southern edge of the ITZC at 4°N, with net change in surface pressure of approximately 2 hPa. There is no indication of a sharp jump in meridional pressure gradient at the location of the rapid increase in surface winds front near 1°N.

Oceanic thermal fronts are often regarded as transitional zones where the ABL must adjust rapidly to a new set of surface boundary conditions. A strong surface gradient in SST combined with cross-frontal winds going from the cold side to the warm side will lead to the development of an unstable ABL. The development of the unstable ABL over the equatorial front is confirmed by six atmospheric soundings that were collected between the equator and 2°S. The two stations located on the cold side of the front clearly indicate a stable boundary layer (Fig. 3). The average stratification is 0.6°C (100 m)$^{-1}$ up through 2500 m. The profile from 0.13°S is stable below 500 m. The profile at 0.28°N is closer to neutral conditions, with a hint of a residual mixing layer near 400 m and slightly weaker stratification near the surface. A trade wind inversion layer is found above about 1000 m.

The ABL on the warm side of the front is observed in the three soundings (Fig. 4). A well-mixed surface layer is observed as a near-uniform layer of potential temperature at each warm side station from the surface up to a height ranging from 350 to 450 m. The average temperature in the well-mixed layer increases to the north in synchronicity with the increase in sea surface temperature. Just below 50 m, there is an increase in mixing ratio that may be caused by spray droplets and ship wake effects. The mixing ratio profiles hint that

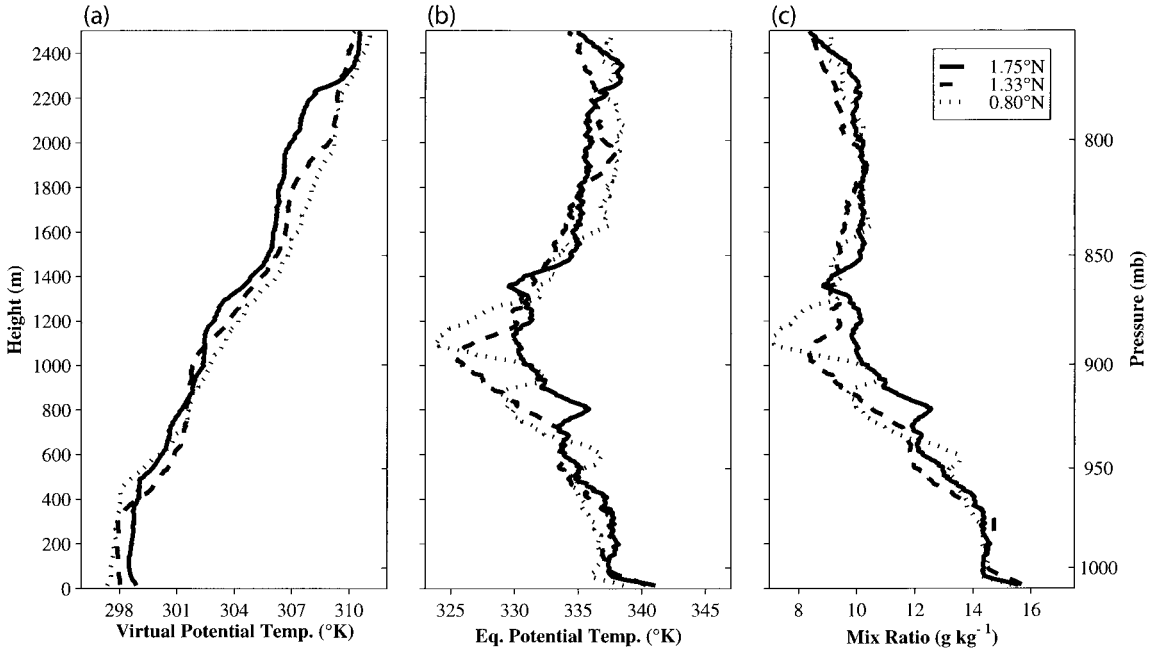

FIG. 4. Boundary layer profiles from warm side of the equatorial front. (a) Virtual potential temperature, (b) equivalent potential temperature, and (c) mixing ratio for three profiles located along 125°W at 0.80°, 1.33°, and 1.75°N.

the height of the unstable ABL is smaller at 0.8°N than at 1.33°N and 1.75°N; however, this result is uncertain and may just be an indication of diurnal and turbulent variability. Note also that there is a significant change in the thermodynamic structure above 500 m going from the cold side to the warm side of the front.

The zonal surface winds change rapidly from -2 to -6 m s^{-1} over the 55 km between the stations at 0.28° and 0.8°N. This change is concurrent with the rapid formation of the unstable ABL. Most of the acceleration in the zonal wind occurs over 55 km between the stations at 0.8° and 1.33°N. The collocation of the development of the unstable ABL with the rapid acceleration of the surface winds is consistent with the Wallace et al. (1989) hypothesis that the convective boundary layer mixes down momentum from a low-level jet. It is puzzling that the acceleration of the zonal winds happens prior to the acceleration of the cross-frontal component. The result is that the maximum in wind stress curl occurs prior to the maximum in wind stress divergence. Unfortunately, without coincident wind profiles, I cannot provide a satisfactory explanation for this incongruity or explicitly confirm the hypothesis of Wallace et al. (1989).

4. Discussion

There has been little theoretical work on the development of unstable ABL over oceanic fronts. Venkatram (1977) suggests a theoretical formula for the height of the internal boundary layer (IBL) generated by a thermal front. Venkatram (1977) assumes a discrete jump in the surface temperature; however, the observed front has a near-constant change in SST over 150 km. Also, Venkatram's (1977) formula would suggest the IBL height grows downwind of the front; however, these observations show the IBL is forming within the front, and there is no clear evidence of the height growing. In addition, the choice of a constant entrainment coefficient may be inappropriate for this case because there may be significant shear at the top of the mixed layer, driving added entrainment. So it is clear that the IBL height from this theory is not completely appropriate. However, it is instructive to use his theory as an example, as Hsu (1984) did for the case of the warm Kuroshio Current.

As implemented by Hsu (1984), Venkatram's (1977) formula states that

$$h = \left[\frac{2C_d(\theta_{\text{warm}} - \theta_{\text{cold}})X}{\gamma(1 - 2F)}\right]^{1/2}, \qquad (1)$$

where h is the height of the IBL, C_d is the drag coefficient, θ_{warm} and θ_{cold} are the temperatures on the warm and cold sides of the front, X is the distance downwind of the front, γ is the lapse rate above the boundary layer and downwind, and F is an entrainment coefficient. An expected IBL height can be calculated using the cross-frontal surface observations. For example, consider the observed front between 0.5° and 1.5°N. For this case, the cross-frontal temperature difference is 4°C and the cross-frontal distance is 100 km. The upwind lapse rate, measured on the cold side of the front, is 0.0096°C m^{-1}. The drag coefficient is taken as 0.0012 (Large and Pond 1981). Hsu (1984) suggests using an entrainment co-

efficient of 0.2 for a convective boundary layer after Driedonks (1982). This example yields an expected IBL height of 355 m near 1.5°N, which is in approximate agreement with the observations, although theory is not completely applicable to this case. Hsu (1984) used this same analysis for a pair of profiles taken across the Kuroshio Current front that was much sharper than the equatorial front. For an across-front SST change of 2.7°C and a width of 15 km, Hsu (1984) calculated a layer height of 150 m that was in good agreement with his observations.

There have been other studies that have examined the abrupt surface wind speed changes across oceanic fronts (Sweet et al. 1981; Rouault et al. 2000; Vihma et al. 1998). A noteworthy one is that of Sweet et al. (1981), who studied the ABL over the north wall of the Gulf Stream. They examined wind, temperature, and humidity soundings collected by aircraft over two days. They found very abrupt surface wind speed changes from less than 5 to 15 m s^{-1} moving from the cold side to the warm side of the front while the low-level winds were steady above 250 m. The wind speed change occurred over less than 1 km as detected by visual and radar imagery of surface roughness. This was a shorter scale than the width of SST front. They then confirmed the rapid change in surface winds by dropping smoke flares on either side of the transition region. The modification of surface wind speed was attributed to the transition in ABL stability across the front and turbulent entrainment of low-level winds to the surface.

Chelton et al. (2001) studied the surface wind vector and its links to the SST gradient vectors using QuikSCAT scatterometer and TMI data. One of their findings shows a stronger response of wind stress divergence to downwind SST gradient than wind stress curl to crosswind SST gradient. They suggest this might be an indication of a finite boundary layer response time yet there is no direct ABL data available to confirm this hypothesis. The spatial resolution of the TMI SST is 46 km, and QuikSCAT surface wind is 25-km resolution, yet this may not be sufficient to resolve fully the rapid transitions in these fields. The scatterometer was not in operation during September of 1998 so no direct comparison with the in situ observations is possible.

There is a hint, at the southernmost end of the transect, of an increase in winds that indicates a southeasterly trade wind regime to the south of 2°S. The surface winds decelerate and converge as they enter the cold tongue. Although Wallace et al. (1989) focused on the northern front, the observation of stronger winds over warmer water to the south of the cold tongue is consistent with their hypothesis that boundary layer stability controls the strength of surface winds. These observations are also consistent with Chelton et al. (2000), who clearly show the deceleration and associated convergence of the surface winds over the southern front using QuikSCAT data.

5. Conclusions

Oceanic thermal fronts are often regarded as transitional zones where the ABL must adjust rapidly to a new set of surface boundary conditions. The new observations indicate an unstable ABL may form above the north wall of the cold tongue during the cold season of a cold-year event when the meridional gradients are the strongest in the eastern tropical Pacific. A stable boundary layer was observed over the cold tongue. The equatorial front on the north wall of the cold tongue extended for 150 km from 0.4° to 2°N and had a constant SST gradient. The unstable ABL was observed throughout this region, with a height between 350 and 450 m. The formation of this unstable ABL occurred within 50 km of the center of the cold tongue and was collocated with a rapid acceleration of the surface winds. This is consistent with the Wallace et al. (1989) hypothesis that stability-dependent boundary layer effects might control surface winds.

The observed change in surface wind speed at the front occurred over just a fraction of the total width of the equatorial front. This result is similar to abrupt surface wind modification observed at times over other oceanic fronts (Sweet et al. 1981). Thus, the scale of surface wind divergence and curl may be much smaller than the corresponding SST gradients and may not be fully resolved by remote sensing and general circulation models.

The equatorial front may not be such a unique place. Modification of surface winds has been studied at several marine fronts, including the Gulf Stream (Sweet et al. 1981), the Agulhas front (Rouault et al. 2000), and the Denmark Strait (Vihma et al. 1998), and several models have been developed to study the ABL and surface wind modification over these marine fronts (e.g., Huang and Raman 1988). The unique aspect of the equatorial front problem is the open-ocean and low-latitude setting. The implementation of an appropriate model to examine the ABL more closely over the equatorial front may help us to understand better the stability-dependent boundary layer effects on the air–sea coupling in this climatologically important region.

Acknowledgments. S. Chen and P. Minnett supported the atmospheric sounding operations during the PACS mooring cruise and R. Weller is my Coinvestigator on the PACS surface mooring project. Thoughtful discussions with C. Zhang and T. Vihma provided initial motivation for this analysis. D. Chelton and S. Esbensen provided helpful comments on the manuscript. D. Chelton and M. Schlax provided the TMI SST figure constructed from TMI data provided by F. Wentz and C. Gentemann of Remote Sensing Systems, Inc. The WHOI Upper Ocean Processes Group along with E. Key (University of Miami) assisted in the data collection at sea. The captain and crew of R/V *Melville* are thanked for their help and skillful ship operations. This work

was supported by the National Oceanic and Atmospheric Administration Office of Global Programs under Contracts NA66GPO130 and NA96GPO428.

REFERENCES

Bond, N. A., 1992: Observations of planetary boundary layer structure in the eastern equatorial Pacific. *J. Climate,* **5,** 699–706.

Chelton, D. B., F. J. Wentz, C. L. Gentemann, R. A. de Szoeke, and M. G. Schlax, 2000: Microwave SST observations of transequatorial tropical instability waves. *Geophys. Res. Lett.,* **27,** 1239–1242.

——, and Coauthors, 2001: Observations of coupling between surface wind stress and sea surface temperature in the eastern tropical Pacific. *J. Climate,* **14,** 1479–1498.

Deser, C., J. J. Bates, and S. Wahl, 1993: The influence of sea surface temperature gradients on statiform cloudiness along the equatorial front in the Pacific Ocean. *J. Climate,* **6,** 1172–1180.

Driedonks, A. G. M., 1982: Sensitivity analysis of the equations for a convective mixed layer. *Bound.-Layer Meteor.,* **22,** 475–480.

Hayes, S. P., M. J. McPhaden, and J. M. Wallace, 1989: The influence of sea-surface temperature on surface wind in the eastern equatorial Pacific: Weekly to monthly variability. *J. Climate,* **2,** 1500–1506.

Hsu, S. A., 1984: Effect of cold-air advection on internal boundary-layer development over warm oceanic currents. *Dyn. Atmos. Oceans,* **8,** 307–319.

Huang, C.-Y., and S. Raman, 1988: A numerical modeling study of the marine boundary layer over the Gulf Stream during cold air advection. *Bound.-Layer Meteor.,* **45,** 251–290.

Large, W. G., and S. Pond, 1981: Open ocean momentum flux measurements in moderate to strong winds. *J. Phys. Oceanogr.,* **11,** 324–336.

Legeckis, R. W., 1977: Long waves in the eastern tropical Pacific Ocean: A view from a geostationary satellite. *Science,* **197,** 1179–1181.

Lindzen, R. S., and S. Nigam, 1987: On the role of sea-surface temperature gradients in forcing low-level winds and convergence in the Tropics. *J. Atmos. Sci.,* **44,** 2418–2436.

Mitchell, T. P., and J. M. Wallace, 1992: The annual cycle in equatorial convection and sea surface temperature. *J. Climate,* **5,** 1140–1156.

Ostrom, W., B. Way, S. Anderson, B. Jones, E. Key, and G. Yuras, 1999: Pan American Climate Study (PACS) mooring deployment cruise report. R/V *Melville* Cruise PACS03MV, WHOI Tech. Rep. WHOI-99-06, 74 pp. [Available from Data Library and Archives, MS 8, Woods Hole Oceanographic Institution, Woods Hole, MA 02543.]

Pullen, P. E., R. L. Bernstein, and D. Halpern, 1987: Equatorial longwave characteristics determined from satellite sea surface temperature and in situ data. *J. Geophys. Res.,* **92** (C1), 742–748.

Rouault, M., A. M. Lee-Thorp, and J. R. E. Lutjeharms, 2000: The atmospheric boundary layer above the Agulhas Current during alongcurrent winds. *J. Phys. Oceanogr.,* **30,** 40–46.

Sweet, W., R. Fett, J. Kerling, and P. LaViolette, 1981: Air–sea interaction effects in the lower troposphere across the north wall of the Gulf Stream. *Mon. Wea. Rev.,* **109,** 1044–1052.

Venkatram, A., 1977: A model of internal boundary-layer development. *Bound.-Layer Meteor.,* **11,** 419–437.

Vihma, T., J. Uotila, and J. Launianinen, 1998: Air–sea interaction over a thermal marine front in the Denmark Strait. *J. Geophys. Res.,* **103** (C12), 27 665–27 678.

Wallace, J. M., T. P. Mitchell, and C. Deser, 1989: The influence of sea surface temperature on surface wind in the eastern equatorial Pacific: Seasonal and interannual variability. *J. Climate,* **2,** 1492–1499.

Warner, T. T., M. N. Lakhtakia, J. D. Doyle, and R. A. Pearson, 1990: Marine atmospheric boundary layer circulations forced by Gulf Stream sea surface temperature gradients. *Mon. Wea. Rev.,* **118,** 309–323.

Xie, S.-P., M. Ishiwatari, H. Hashizume, and K. Takeuchi, 1998: Coupled ocean–atmosphere waves on the equatorial front. *Geophys. Res. Lett.,* **25,** 3863–3866.

Yin, B., and B. A. Albrecht, 2000: Spatial variability of atmospheric boundary layer structure over the eastern equatorial Pacific. *J. Climate,* **13,** 1574–1592.